Retrieval of Snow Properties for Ku- and Ka-band Dual-Frequency Radar

Liang Liao[1], Robert Meneghini[2], Ali Tokay[3] and Larry F. Bliven[4]

[1] Goddard Earth Science Technology & Research, Morgan State University, MD

[2] NASA Goddard Space Flight Center, Greenbelt, MD

[3] University of Maryland Baltimore County/JCET, MD

[4] NASA Wallops Flight Facility, VA

Submitted to

Journal of Applied Meteorology and Climatology

Corresponding author information:

Dr. Liang Liao
Goddard Earth Sciences Technology and Research
Morgan State University
Code 612
NASA/Goddard Space Flight Center
Greenbelt, MD 20771

301-614-5718 (phone)
301-614-5492 (fax)
Email: Liang.Liao-1@ nasa.gov

Abstract

The focus of this study is on the estimation of snow microphysical properties and the associated bulk parameters such as snow water content and water equivalent snowfall rate for Ku- and Ka-band dual-frequency radar. This is done by exploring a suitable scattering model and the proper particle size distribution (PSD) assumption that accurately represent, in the electromagnetic domain, the micro/macro-physical properties of snow. The scattering databases computed from simulated aggregates for small to moderate particle sizes are combined with a simple scattering model for large particle sizes to characterize snow scattering properties over the full range of particle sizes. With use of the single scattering results, the snow retrieval look-up tables can be formed in a way that directly links the Ku- and Ka-band radar reflectivities to snow water content and equivalent snowfall rate without use of the derived PSD parameters. A sensitivity study of the retrieval results to the PSD and scattering models is performed to better understand the dual-wavelength retrieval uncertainties. To aid in the development of the Ku- and Ka-band dual-wavelength radar technique and to further evaluate its performance, self-consistency tests are conducted using measurements of the snow PSD and fall velocity acquired from the Snow Video Imager/Particle Image Probe (SVI/PIP) during the winter of 2014 in the NASA Wallops flight facility site in Wallops Island, Virginia.

1 Introduction

The Global Precipitation Measurement (GPM) core satellite, a joint Earth-observing mission between the National Aeronautics and Space Administration (NASA) and the Japan Aerospace Exploration Agency (JAXA), was successfully launched into orbit on 27 February of 2014 from Japan (Hou et al. 2008 and 2014). One of the goals of the Dual-frequency Precipitation Radar (DPR) aboard the GPM satellite is to provide measurements and estimates of snow precipitation rate and water content for mid- and high-latitude regions. This is usually done by estimating parameters of snow particle size distribution (PSD) that are often modeled by an analytical function, such as the exponential, gamma or lognormal distribution, with two or three unknown parameters (Gorgucci et al. 2000 and 2002; Bringi et al. 2002). The inability of the modeled PSD to represent actual snow spectra and to characterize their intrinsic variations in time and space can lead to errors in the estimates of precipitation rate obtained from the DPR. Additionally, uncertainties associated with scattering computations of snow aggregates also affect the accuracy of the dual-wavelength radar retrieval of snow arising from the complex shape and structure of snow aggregates and the corresponding variability in the scattering parameters. Therefore, understanding the uncertainties in snow precipitation estimation that depend on PSD parameterizations and scattering models of individual particles is important in evaluating the overall performance of DPR retrieval algorithms and in gaining insight into ways to improve the algorithms.

Several studies have been carried out using dual-frequency radar for the retrieval of precipitating ice/snow parameters from the ground (Matrosov 1998; Szyrmer and Zawadzki 2014) and from airborne radar measurements (Liao et al. 2005, 2008; Heymsfield et al. 2005; Wang et al. 2005;

Matrosov et al. 2005). Although various combinations of frequencies were used in these studies, a common feature is that at least one of the radar frequencies operates in the non-Rayleigh regime to ensure a measurable difference in the reflectivities. It is this differential reflectivity that can be related to a characteristic size parameter of the snow particle distribution. Because of uncertainties in the snow microphysics arising from the natural variability of the particle density, shape, and orientation and also because of uncertainties associated with the particle backscattering cross section and terminal fall velocity as well as the natural variability in PSDs, it is important to assess the errors in the model and their impacts on the retrievals.

The emphasis of this study is on the estimation of snow microphysical properties and the associated bulk parameters such as snow water content and water equivalent snowfall rate. As indicated earlier, one of the challenges in the radar retrieval of snow is to characterize the variability of the snow PSD and to efficiently compute scattering properties of the snowflakes over the full range of sizes. The aim of our study is to explore a suitable scattering model and an appropriate PSD that accurately represents, in the electromagnetic domain, the micro/macro-physical properties of snow.

Although several scattering databases are available, which provide the scattering properties of snow aggregates (Liu 2004 and 2008; Nowell et al. 2013; Kuo et al. 2016), they are often limited to small-to-moderate particle sizes for a limited set of frequencies. These limitations arise not only because of the magnitude of the computational burden but also because of the convergence properties of the numerical solution. To develop an operational-type radar algorithm for the DPR snow retrieval, it is desirable to have a scattering model that provides efficient computation at an

arbitrary frequency over a large range of particle sizes. Comparisons of the scattering results between simple and more complicated snow models indicate that the scattering properties of aggregates at the DPR frequencies are fairly well reproduced by randomly-oriented ellipsoidal particles if the effective mass density of snow is constant with size (Liao et al. 2013). By taking advantage of both developed scattering databases and simple scattering models, we attempt to employ the scattering results of the aggregates from the scattering database for small to moderate particle sizes and use the results from the simple scattering models for large particles to cover the full range of particle sizes for characterizing snow scattering properties at Ku- and Ka-band.

One of the DPR algorithms for snow retrieval employs a fixed-snow-density spherical model for computations of the Ku- and Ka-band radar backscattering and extinction cross sections using the assumption of an exponential PSD (Seto et al. 2013). To improve snow retrieval accuracy, we will investigate retrieval uncertainties associated with the PSD and the particle scattering models, and introduce new forms of the retrieval look-up tables that directly link DPR Ku- and Ka-band radar reflectivities to snow water content and snowfall rate without the use of derived PSD parameters. Newly formed look-up tables provide an effective means not only for snow retrieval but for analysis of the retrieval uncertainties associated with the PSD model and the particle scattering models. In order to check the consistency of the snow retrievals, measurements of the snow PSD and fall velocity acquired from the Snow Video Imager/Particle Image Probe (SVI/PIP) are used (Newman et al. 2009). It is believed that a collection of long-term PSD data, fall velocities and information on particle mass spectra will provide a strong basis for evaluating the performance of the DPR Ku- and Ka-band techniques.

This article is organized as follows. Methods for snow retrieval are described in Section 2, and measurements of the PSD are discussed in Section 3, followed by remarks and a summary in Section 4.

2 Technical Approach and Methodology

Understanding the retrieval errors associated with the snow particle size/mass distributions models and particle scattering models employed by the DPR algorithms is important for the evaluation of algorithm performance. The study also provides insight into which of the models yield the most accurate DPR estimates of snow. Proper selection of the PSD and scattering models can improve the overall performance of the DPR profiling algorithm. What follows are discussions of snow scattering models and the parameterization of the particle size spectra and how these models affect the radar retrievals.

2.1 Single scattering model of snow aggregates

Several simulated aggregate models have been developed using the pristine ice crystal habits found in nature as the basic elements from which the aggregates are constructed (Draine and Flatau 1994; Liu 2004 and 2008; Weinman and Kim 2007; Petty and Huang 2010; Botta et al. 2010 and 2011; Nowell et al. 2013; Kuo et al. 2016). For these particles, a numerical scheme is required to compute the scattered fields. Although these numerical computations are useful, they are time consuming, and are often limited to small-to-moderate particle sizes for a limited set of frequencies. A few scattering databases derived from simulated aggregates are available (Nowell et al. 2013; Kuo et al. 2016), but the maximum equivalent ice diameter is limited to around 2.5-3 mm which is not large enough to cover entire particle size range.

144

145 To account for the scattering contribution from the entire particle size range, the current DPR
146 algorithms adopt a simple scattering model, namely, the ice-air mixed spheres with a fixed snow
147 density of 0.1 g/cm^3 for all particle sizes (Seto et al. 2013). To check the validity and accuracy of
148 the simple geometric scattering model, a study was carried out by Liao et al. (2013) in which
149 scattering results from aggregates comprised of 6-branch bullet rosette crystals were compared
150 with those obtained from spherical or spheroidal ice-air mixed phase particles. Shown in Fig.1 is
151 an example of these results, in which backscattering (left) and extinction (right) coefficients at
152 35.6 GHz are plotted versus the equivalent ice diameter for 3 simulated snow aggregates and
153 results from the sphere, oblate and prolate spheroids. A constant effective snow density of 0.2
154 g/cm^3 is assumed for all spherical and spheroidal particle models. The spheroids are assumed to
155 be randomly oriented, i.e., their symmetry axes are uniformly distributed in three-dimensional
156 space. The aspect ratios (γ) of the spheroids, defined as the ratio of polar to equatorial lengths,
157 are taken to be either 0.5 or 2 to represent oblate and prolate spheroids respectively. The results
158 of the study show that the scattering properties of the aggregates are fairly well reproduced by an
159 equivalent-mass spheroidal particle when a constant snow density is assumed.
160

161 Agreement between the spheroidal/fixed density model and the aggregates suggests the validity
162 of the simple model and its utility for computing look-up tables for the DPR. An effective snow
163 density of 0.2 g/cm^3 is best able to reproduce the scattering parameters of the bullet-rosette
164 aggregates at the DPR frequencies. It is important to note that the effective mass density, as
165 defined in this paper, is that mass density of a spheroidal particle whose associated scattering
166 parameters provide the best match to those of the simulated aggregates with the same mass. This
167 definition is motivated by the desire to match the scattering properties of the spheroidal and

simulated aggregates and is distinct from the usual definition of snow density given by the ratio of the particle mass to the volume where the volume is taken to be that of a circumscribing sphere or spheroid. To distinguish our definition from others, the density we use for scattering computations is referred to as the effective snow density. It is also important to note that the snow mass is preserved in both definitions; that is, the product of the mass density or effective mass density and the particle volume yields the same mass.

Recently, Kuo et al. (2016) have developed a comprehensive scattering database, which is computed using the discrete dipole approximation (DDA) from a collection of realistic aggregates simulated from a 3-D growth model with mass vs. size and fractal properties that are consistent with field observations (Gravner and Griffeath 2009). Because of its limited range of particle size mentioned earlier, the scattering tables of snow aggregates in our study will be taken as a hybrid form that combines the scattering results from the Kuo et al. scattering database for small to moderate particle sizes and the results from the simple scattering models for large particles. Illustrated in Figs.2 and 3 are these scattering results at Ku- and Ka-bands from the Kuo et al. database along with the results from an oblate spheroidal model for particle diameters up to 6 mm. The results from the simple models (red curves) are those obtained from the randomly-oriented oblate spheroids with an aspect ratio of 0.7 and a constant effective mass density of 0.2 g/cm^3. The results of the scattering tables, which are denoted by the term "fitted" and shown by the black curves, represent the mean values of the data from the scattering database, where the mean is taken from all types of aggregates having the same mass, and the results from the 0.2 g/cm^3 oblate spheroid model in the size range where the scattering database is unavailable. The maximum liquid equivalent diameters of the current Kuo et al. database at

191 Ku- and Ka-bands are 3 and 2 mm, respectively. In other words, the scattering results from the
192 simple models are employed in the tables for the size ranges from 3-6 mm at Ku-band and 2-6
193 mm at Ka-band. The fairly good agreement of the scattering results in Figs. 2 and 3 between the
194 simple model and the scattering database (with mean differences less than 10% for the
195 backscattering and 7% for extinction cross sections) over the size range where the database is
196 valid suggests the validity of the simple models for the smaller particle sizes. As the scattering
197 database is updated to cover larger particle sizes, the validity of the simple scattering model will
198 be reassessed.
199
200 2.2 Particle size/mass distribution model
201
202 The three-parameter gamma distribution is one of the most common ways to mathematically
203 describe hydrometeor size/mass distributions (Gorgucci et al. 2000 and 2002; Bringi et al. 2002).
204 The form of the gamma distribution is expressed as

205 $$N(D) = N_W f(\mu)\left(\frac{D}{D_m}\right)^{\mu} \exp(-\Lambda D), \quad (1)$$

206 where D_m is the mass-weighted diameter of the particle, N_w is a scale factor, and μ is the shape
207 factor where

208 $$f(\mu) = \frac{6(4+\mu)^{\mu+4}}{4^4 \Gamma(\mu+4)} \quad \text{and} \quad \Lambda = (4+\mu)/D_m, \quad (2)$$

209 To describe snow particle size and mass spectra, the PSD in (1) and (2) is given as a function of
210 liquid equivalent or melted diameter D, which is also called particle melted-size distribution. D_m
211 is the melted median mass diameter, defined by
212

213 $$D_m = \frac{\int_0^\infty D^4 N(D) dD}{\int_0^\infty D^3 N(D) dD}. \quad (3)$$

214

215 In the inner swath, the DPR provides Ku- and Ka-band reflectivity factor measurements at each
216 range gate so only two parameters of the PSD can be determined. Typically, the shape factor (μ)
217 is taken to be constant. Although μ is often set to zero (exponential distribution) (Gunn and
218 Marshall 1958; Seto et al. 2013), the impact of this choice on the retrieval needs to be
219 investigated.

220

221 The differential frequency ratio (DFR), which is defined as the difference between the radar
222 reflectivity factors at Ku- and Ka-bands in decibels, is perhaps the most important quantity for
223 the dual-wavelength radar techniques in estimating hydrometeor micro/macro-physical
224 properties. As the DFR is independent of N_w, D_m can be derived from the DFR relations once μ
225 has been fixed. However, the DFR-D_m relation depends not only on μ but on the particle shape,
226 orientation distribution and mass density. Fig.4 provides the results of DFR as a function of the
227 liquid equivalent median mass diameter using a randomly-oriented, fixed density spheroidal
228 particle model. The left plot shows the variations in the DFR-D_m relation resulting from
229 different effective snow densities. Computations of the radar scattering parameters at different
230 effective snow densities are made in the same way as in the case of 0.2 g/cm^3. The particle sizes
231 (semi axes of spheroid) are solely determined by the density specified for a given particle mass.
232 The center plot shows the effects of particle shape where a γ value of 1 corresponds to a sphere
233 while γ values less than 1 correspond to an oblate spheroid. The plot on the right shows the
234 effect of changing μ. Analysis of these results indicates that particle shape has a small effect on

235 the DFR-D_m relation and changes the results by less than 4% for changes in γ from 0.5 to 1 while
236 the shape factor leads to the change in the results of no more than 20%. On the other hand, the
237 DFR-D_m relation has a strong dependence on the effective snow density. In other words, the
238 determination of D_m from the DFR is relatively insensitive to μ and to particle shape, if the
239 orientation is random, whereas the relationship is quite sensitive to the effective snow density
240 used for computations of the scattering parameters. As can be seen in Figs.1-3, the extinction
241 coefficients at both Ku- and Ka-bands, though in good agreement between the simple model and
242 the scattering database, are small and can usually be neglected. It should be noted that the above
243 conclusions are based on the assumption of random orientation of the aggregates. When this
244 assumption is violated, then the orientation distribution as well as particle shape become
245 important.
246
247 Although an effective snow density of 0.2 g/cm^3 is found to be suitable for the computations of
248 the Ku- and Ka-band radar scattering parameters for equivalent ice diameters up to 2-3 mm,
249 further testing will be necessary to assess this assumption when scattering results from larger
250 aggregates become available. It is worth noting that the results of Liao et al. (2013) show
251 reasonably good agreement between radar scattering parameters at higher frequencies (from 89-
252 183.31 GHz) as derived from the simple models and the simulated aggregates for particle
253 diameters up to 2.5 mm despite the fact that the simple models using spheres or nearly spherical
254 particles produce backscattering results with more pronounced oscillations (resonance effects)
255 than the aggregate results. This is encouraging in the sense that it shows that an effective density
256 of 0.2 g/cm^3 yields good agreement with the simulated aggregate results for electrically larger
257 particles. On the other hand, it might be the case that the effective snow density may need to be

changed for larger particle types so as to ensure good agreement. In either case, the objective is to provide scattering tables at all relevant frequencies and particle sizes that incorporate the most recent scattering results.

2.3 Dual-wavelength retrieval algorithm

As discussed above, D_m can be derived from the DFR-D_m relations for a given μ. In principle, once D_m is determined, N_w is derived using the radar reflectivity at either Ku- or Ka-band. Subsequently, snow water content (SWC) and equivalent snowfall rate (R_S) can be computed from the derived PSD parameters. The fall velocity of snow is needed in order to estimate R_S. For the development of an effective dual-wavelength radar retrieval technique, it is desirable to employ look-up tables (LUT) that are formed in such a way that the radar measurements are directly linked to the microphysical properties of snow (D_m and N_w) and its associated bulk parameters (SWC and R_S). With use of the LUTs different particle models and their scattering properties can be evaluated separately in the context of the same algorithm.

Illustrated in Fig.5 are such tables in which SWC (top-left), R_S (top-right), D_m (bottom-left) and N_w (bottom-right) along the ordinate are given as a function of the DFR. A flowchart is provided in Fig.6 showing the procedures to compute the radar reflectivitity factors and snow size and bulk hydrometeor parameters from an assumed mass spectrum model. In Fig.5, SWC, R_S, N_w have been normalized by the Ku-band radar reflectivity factor so that they can be expressed solely as a function of DFR for given PSD and scattering models. The way to normalize liquid water content by reflectitities has previously been adopted in the study of ice clouds (Hogan et

al. 2000; Botta et al. 2013). The results in Fig.5 are computed under the assumption that the snow particles are fixed-density, randomly-oriented oblate spheroids with an aspect ratio of 0.7 that follow an exponential particle size distribution. As an example, and also for reference, the tables are plotted in Fig.5 for effective snow densities varying from 0.05 to 0.5 g/cm^3. The terminal velocities of snowflakes used for the computations of R_S are based on the results of Magono and Nakamura (1965). It is important to note that the results from the LUTs shown in Fig.5 can be used to determine SWC and R_S as they directly link the DPR radar reflectivities to SWC and R_S without use of the derived PSD parameters.

The procedure for the estimation of snow parameters is described as follows: given a pair of reflectivity factors (Z_{Ku}, Z_{Ka}), the DFR in dB is defined as $10\text{Log}_{10}(Z_{Ku}/Z_{Ka})$, from which we find the values of SWC/Z_{Ku} (left) and R_S/Z_{Ku} (right) for an assumed effective snow density. By multiplying by Z_{Ku}, the results of SWC and R_S are then obtained. Obviously the values of SWC and R_S depend on the effective snow density. The estimates of D_m and N_w can be achieved in a similar way. It is worth mentioning again that snow attenuations, though correctable, are typically negligibly small for most Ku- and Ka-band spaceborne radar measurements.

As LUTs change with different scattering models and PSD parameterizations, a proper selection of the tables is critical to the accuracy of the retrieval. It is instructive to conduct a sensitivity study with respect to the model assumptions and to gain an understanding of the uncertainties associated with each of the models. Figure 7 provides such a sensitivity study in which the LUTs are checked against 3 μ values. Similar to the findings in Fig.4, a change in μ leads to changes in the estimates of SWC and R_S of less than 20% so that the assumption of μ equal to zero, as found

304 in many observations, yields a reasonable approximation for the estimates of snow. Although it
305 is worth testing the scattering databases of the aggregates formed from various crystal habits, it is
306 not the focus of the study to evaluate and validate these scattering databases. Because the mass
307 of the aggregates is the dominant factor in the scattering parameters at Ku- and Ka-bands,
308 significant differences among the various scattering databases are not expected. This is
309 evidenced by the fact of that there is good agreement between the scattering databases derived by
310 Nowell et al. (2013) and Kuo et al. (2016) and that the small variations of the scattering and
311 extinction coefficients as computed from various aggregate models (Kuo et al. 2016) can be seen
312 from the variations in the data (blue) shown in Figs.2-3.
313
314 **3 Assessment of snow retrieval: PSD model assumptions**
315
316 Because of the complexity of snowfall processes and the difficulties encountered in accurately
317 measuring the microphysical properties, validating snow estimates is a challenging task. With the
318 advent of more advanced digital cameras and image processing technologies, measurements of
319 falling snow have been improved to the point where the snow particle size spectra and fall
320 velocities can be obtained fairly accurately (Bohm 1989; Huang et al. 2010 and 2015; Garrett et
321 al. 2012). An independent and direct measurement of the mass of individual snow particles is,
322 however, still a difficult task, and therefore direct measurements of the snow mass spectrum are
323 rarely available. Several investigations into deriving snow mass spectra are being pursued, which
324 are in fact part of the effort in the GPM ground validation project. These methods are based on
325 the principle that particle masses can be related to their fall velocities after accounting for air
326 drag and other aerodynamics effects (Bohm 1989; Heymsfield et al. 2010). Understanding the
327 microphysical properties of snow should further improve our ability to generate better scattering

representations and more accurate look-up tables for retrieving snow bulk properties from the DPR. It would be ideal to evaluate snow retrievals with co-located dual-wavelength radar measurements and in situ snow microphysical measurements. These data, though desirable, are not available. Our attention is therefore focused on the assessment of the PSD assumptions used in developing the retrieval algorithms using measured PSD.

To check the consistency of snow retrievals using the LUTs, measurements of snow spectra are used. The data were obtained from 8 snow events during winter of 2014 taken at the NASA Wallops Flight Facility in Wallops Island, Virginia using the Snow Video Imager/Particle Image Probe (SVI/PIP). Table 1 provides details of these events that include starting and ending times of snowfall, mean temperature as well as total accumulations of each event. In Wallops Island annual mean snowfall is about 200.66 mm, and in 2014 it was recorded to be 223.66 mm, slightly more than average. Although the PIP measures the dimensions or sizes of the snowflakes and their fall velocities, it does not provide measurements of particle mass. In order to compute the radar reflectivities and snow bulk parameters as in (4) and (5), the mass spectra or melted size spectra are needed. Conversion of the PSD measurements to the mass spectra, however, relies on the empirical mass-size relations. There are many such relationships available in the literature that can be used to derive m(D) (Nakaya 1954; Magono and Nakamura 1965; Zikmunda and Vali 1972; Locatelli and Hobbs 1974; Mitchell et al. 1990; Brandes et al. 2007; Heymsfield et al. 2010). These results show some variability depending on snow type, amount of riming and other conditions under which the measurements were made. In this study, two well-known mass-size relations, the results from Heymsfield et al. (2010) and Brandes et al. (2007), are used to test how the estimates of snow change with use of different mass-size relations when the same LUTs are used.

351

352 An example of the PSD measurements is shown in Fig.8, in which N(D) of the PSD (top), shown
353 along the vertical with the amplitude of the spectrum given by the color scale, is given as a
354 function of time. The equivalent snowfall rate (middle) and median mass diameter (D_m) (bottom)
355 are also shown for the same time period. For the computations of snowfall rate and D_m, empirical
356 snow mass-size relations are used in conjunction with the measured snow particle size spectra
357 and fall velocities. The following equations are used for obtaining R_S and D_m:

358 $$D_m = \frac{\int_0^\infty D\, m(D)N(D)dD}{\int_0^\infty m(D)N(D)dD}, \quad (4)$$

359 $$R_S = \frac{36\times10^{-4}}{\rho_w}\int_{D_{min}}^{D_{max}} N(D)\, m(D)V(D)dD, \quad (5)$$

360 where D and D_m in (4) and (5) as well as in Fig.8 are, respectively, the actual particle diameter
361 and median mass diameter rather than the melted sizes employed in the rest of the paper. m(D)
362 is the particle mass-size relation, and ρ_w is the water mass density taken to be 1 g/cm^3. Note also
363 that the data shown in Fig. 8 represent a measurement period of 1000 minutes of snow data
364 (~three snow events) with a one-minute integration time. The mass-size relation of Heymsfield et
365 al. (2010) is used for computations of R_S and D_m.

366

367 Illustrated in Fig.9 are the scatter plots (red dots) of SWC (top row) and R_S (bottom row)
368 computed from the measured PSD with use of mass-size relations when the hybrid scattering
369 tables are assumed. For reference, the LUTs derived from the constant effective density
370 scattering models as shown in Fig.6 are superimposed in Fig.9. The SWC and R_S as well as the
371 quantities associated with the Ku- and Ka-band radar reflectivities shown in Fig.9 are obtained
372 from a total of about 8000 1-minute PSD measurements collected from the PIP during the winter

373 of 2014 at Wallops using the mass-size relations of Brandes et al. (left column) and Heymsfield
374 et al. (right column). Mass-size relations are used to convert the measured particle size
375 distribution (PSD) to the melted size distribution from which the scatterings and snow bulk
376 parameters can be computed as in (2)-(5). The mass-size relations used in Fig.9 are those from
377 Eq.(8) of Brandes et al. (2007) and Eq.(10) of Heymsfield et al. (2010). The procedures used in
378 obtaining the radar parameters and SWC and R_S from the measured PSD are shown in the flow
379 diagram of Fig.10. Analysis of the SWC results indicates that the snow water content derived
380 from the measured PSD agree reasonably well with those from the tables when the effective
381 snow density is taken to be 0.2 g/cm^3. Because the scattering table, which is a hybrid formed
382 from the mean aggregate solution at small particle sizes with the spheroidal particle model at
383 larger sizes, used for computing the reflectivities of the measured PSD and the scattering results
384 with a density of 0.2 g/cm^3 are nearly the same as shown in Figs.2-3, the differences in snow
385 water content between the measured PSD and the table results from a density of 0.2 g/cm^3 are
386 mostly caused by the differences between measured and modeled melted particle size
387 distributions. As noted earlier, the exponential melted-size distribution is assumed in the look-up
388 tables while the measured melted-size distribution is derived from the measured particle diameter
389 spectrum and the mass-size relation that generally will be different from an exponential
390 distribution. Computation of the snowfall rate, on the other hand, depends not only on the
391 particle mass (or melted-size) spectrum but also on the particle fall velocities. Most of the
392 estimated snowfall rates, as derived from the measured PSD and the mass-size relations, and
393 shown in the lower panels of Fig.9, lie between the table results with effective densities of 0.1
394 and 0.2 g/cm^3. The mean differences of the SWC between the 0.2 g/cm^3 snow density LUTs and
395 the PSD-derived results are about 20% for Ku-band radar reflectivities greater than 15 dBZ (the

approximate minimum detectable signal of the DPR Ku-band channel). Larger differences between the R_S estimates are found, and can be attributed to differences in the snow fall velocity spectra between the measured and modeled mass distribution. The terminal velocities of snowflakes used for the computations of the LUTs are based on the results of Magono and Nakamura (1965) while the measured fall velocities are used for the computations of PSD snowfall rate.

The overall agreement of the snow water content between the results from the measured PSD and the results from the LUTs suggests that the exponential particle distribution model assumed in the tables is reasonable. Different mass-size relations lead to different mass spectra for a given measured PSD. That the retrieval results from the Brandes et al. and Heymsfield et al. mass-size relations follow the trends of SWC and R_S similar to those derived from the LUTs further suggest that the Ku- and Ka-band dual-wavelength techniques adopted are relatively insensitive to the choice of either the Brandes or the Heymsfield mass-size relation. These results approximately yield the table values obtained from the 0.2 g/cm^3 snow density. It is also worth mentioning that the results from the measured PSD are relatively insensitive to PSD integration time even though the scatter in the data is slightly reduced if a longer integration is used.

4 Summary

The ultimate goal of this study is to better understand the estimation process in retrieving snow microphysical properties (N_w and D_m) and the associated bulk parameters (SWC and R_S) for improvement of the Ku- and Ka-band dual frequency radar retrieval. This is done by first finding suitable single scattering tables and PSD models and then using this information to construct

420 snow retrieval look-up tables. Presently available scattering databases, though accurate and
421 useful, are limited to small and moderate particle sizes. To extend the results to larger sizes, a
422 simple scattering model that agrees well with the scattering databases at small particle sizes is
423 used. It is found that a snow particle model consisting of randomly oriented oblate spheroids
424 with an effective mass density of 0.2 g/cm^3 yields good agreement with the results from the
425 scattering databases at Ku- and Ka-band. Thus the single-particle scattering database is a hybrid
426 that uses the scattering database for small and moderate particles and a simple randomly oriented
427 oblate with a constant effective mass density of 0.2 g/cm^3 for large particles.
428
429 Using single scattering tables and an assumed PSD model, the Ku- and Ka-band radar
430 reflectivity factors and snow bulk parameters are computed. Thus, the relationships between the
431 results of DFR and SWC and R_S are established to form the dual-wavelength radar retrieval look-
432 up tables. Retrievals of snow water content and snowfall rate, as the primary focus of this study,
433 are therefore achieved by using newly introduced look-up tables that directly link Ku- and Ka-
434 band radar reflectivities to hydrometeor parameters without the use of derived PSD parameters.
435 The look-up tables are formed so that SWC and R_S, both of which are normalized by the Ku-
436 band radar reflectivity factor, are expressed as a function of the differential frequency ratio of
437 Ku- and Ka-bands. The look-up tables offer not only computational advantages but provide
438 direct insight into how the model assumptions impact the retrieval results. The nature of one-to-
439 one relations between the normalized hydrometeor parameters and DFR provides a means to
440 obtain unique solutions of the snow parameters for a given PSD and single scattering model. To
441 understand the uncertainties in the snow estimates associated with the PSD parameterizations
442 and scattering models, a sensitivity study was done, finding that the choice of shape factor of the

443 gamma PSD has only a slight impact on the retrievals. As such, a value of μ of zero, as
444 supported by some observations, should yield reasonable estimates of snow parameters from the
445 perspective of dual-wavelength radar retrieval.
446
447 Self-consistency of the snow retrievals has been checked using measurements of snow PSD and
448 fall velocity acquired from the PIP during the winter of 2014 in Wallops. Among several
449 assumptions that have been examined are conversions to particle mass spectra using different
450 mass-size relations, scattering particle models and snow PSD. Analysis of nearly 8000 1-minute
451 PSD measurements suggests that exponential PSD model (μ=0) is sufficiently accurate for the
452 dual-wavelength radar retrieval of snow bulk parameters. It also indicates that the use of either
453 the Heymsfield or the Brandes mass-size relation yields approximately the same snow estimates.
454 However, these findings should be viewed as preliminary because of the limited data
455 measurements at a single location. Collections of long-term PSD data, fall velocities and
456 information on particle mass spectra at multiple sites will provide further evaluation of the
457 performance of the Ku- and Ka-band radar techniques. Further tests of the scattering tables will
458 be done by comparing the accuracy of the simple particle model against scattering results from
459 larger simulated aggregates, as these results become available.
460
461 **ACKNOWLEDGEMENTS:** This work is supported by Dr. R. Kakar of NASA Headquarters
462 under NASA's Precipitation Measurement Mission (PMM) Grant NNH12ZDA001N-PMM. The
463 authors also wish to thank Mr. Jorel Torres of South Dakota School of Mines & Technology for
464 providing and processing SVI/PIP data, and Dr. Kwo-Sen Kuo of University of Maryland for
465 providing the scattering database.

466

Appendix

List of Symbols and Acronyms

GPM:	Global Precipitation Measurement
DPR:	Dual-frequency Precipitation Radar
NASA:	National Aeronautics and Space Administration
JAXA:	Japan Aerospace Exploration Agency
Ku-band:	Frequency of 13.6 GHz
Ka-band:	Frequency of 35.6 GHz
PSD:	Particle Size Distribution
SVI/PIP:	Snow Video Imager/Particle Image Probe
DDA:	Discrete Dipole Approximation
N(D):	Particle Size Distribution
N_W:	Scale Factor of Particle Size Distribution
μ:	Shape Factor of Gamma Distribution
D:	Particle Diameter
D_m:	Mass-weighted Diameter
Λ:	Slope Parameter
DFR:	Differential Frequency Ratio
SWC:	Snow Water Content
R_S:	Equivalent Snowfall Rate
LUT:	Look-up Table
Z_{Ku}:	Ku-band Radar Reflectivity Factor
Z_{Ka}:	Ka-band Radar Reflectivity Factor
m(D):	Particle Mass as Function of Particle Diameter
V(D):	Particle Fall Velocity
ρ_w:	Liquid Mass Density
ρ_s:	Snow Mass Density
D_{min}:	Minimum Diameter
D_{max}:	Maximum Diameter
f:	Frequency
γ:	Aspect Ratio of Particle

References

Brandes, E., K. Ikeda, G. Zhang, M. Schoenhuber, and R. Rasmussen, 2007: A statistical and physical description of hydrometeor distributions in Colorado snowstorms using a video distrometer. *J. Appl. Meteor. Climat*., **46**, 634-650.

Bohm, H.P., 1989: A general equation for the terminal fall speed of solid hydrometeors. *J. Atmos. Sci.*, **46**, pp. 2419-2427.

Botta, G., K. Aydin, and J. Verlinde, 2010: Modeling of microwave scattering from cloud ice crystal aggregates and melting aggregates: A new approach. *IEEE Geo. Rem. Sens. Lett.*, **7**, 572-576.

Botta, G., K. Aydin, J. Verlinde, A.E. Avramov, A.S. Ackerman, A.M. Fridlind, G.M. McFarquhar and M. Wolde, 2011: Millimeter wave scattering from ice crystal aggregates: Comparing cloud model simulations with X- and Ka-band radar measurements. *J. Geophys. Res.*, **116**, D00T04.

Botta, G., K. Aydin, and J. Verlinde, 2013: Variability in millimeter wave scattering properties of dendritic ice crystals. *J. Quant. Spectrosc. Radiat. Transf.*, **131**, 105-104.

Bringi, V., G. Huang, V. Chandrasekar and E. Gorgucci, 2002: A methodology for estimating the parameters of a Gamma raindrop size distribution model from polarimetric radar data: Application to a squall-line event from the TRMM/Brazil campaign. *J. Oceanic and Atmos. Tech.,* **19**, 633-645.

Draine, B. T., and P. J. Flatau, 1994: Discrete dipole approximation for scattering calculations. *J. Opt. Soc. Am. A.*, **11**, 1491-1499.

Garrett, T. J., Fallgatter, C., Shkurko, K., and Howlett, D., 2012: Fall speed measurement and high-resolution multi-angle photography of hydrometeors in free fall. *Atmos. Meas. Tech.*, **5**, 2625-2633.

Gorgucci, G. Scarchilli, V. Chandrasekar and V. Bringi, 2000: Measurement of mean raindrop shape from polarimetric radar observations. *J. Atmos. Sci*., **57**, 3406-3413.

Gorgucci, E., G. Scarchilli, V. Chandrasekar, and V. Bringi, 2002: Estimation of raindrop size distribution parameters from polarimetric radar measurements. *J. Atmos. Sci.,* **59**, 2373-2384.

Gravner, J., and D. Griffeath, 2009: Modeling of snow-crystal growth: A three dimensional mesoscopic approach. *Phys. Rev. E*, **79**, 011601.

Gunn, K. L. S., and J.S. Marshall, 1958: The distribution with size of aggregate snowflakes. *J. Meteor.*, **15**, 452-461.

Heymsfield, A. J., Z. Wang, and S. Matrosov, 2005: Improved radar ice water content retrieval algorithms using coincident microphysical and radar measurements. *J. Appl. Meteor.*, **44**, 1391–1412.

Heymsfield, A. J., and C. D. Westbrook, 2010: Advances in the estimation of ice particle fall speeds using laboratory and field measurements. *J. Atmos. Sci.,* **67**, 2469–2482.

Heymsfield, A. J., C. Schmitt, A. Bansemer, and C. H. Twohy, 2010: Improved representation of ice particle masses based on observations in natural clouds. *J. Atmos. Sci*., **67**, 3303–3318.

Hogan, R., A. Illingworth, and H. Sauvageot, 2000: Measuring crystal size in cirrus using 35- and 94-GHz radars. *J. Atmos. Oceanic Technol.*, **17**, 27-37.

Hou, A., G. S. Jackson, C. Kummerow, and C. M. Shepherd, 2008: Global precipitation measurement. Precipitation: Advances in Measurement, Estimation, and Prediction, S. Michaelides, Ed., Springer, 131–169.

Hou, A. Y., R. K. Kakar, S. Neeck, A. A. Azarbarzin, C. D. Kummerow, M. Kojima, R. Oki, K. Nakamura, and T. Iguchi, 2014: The global precipitation measurement mission. *Bull. American Meteor. Soc*., **95**, 701-722.

Huang, G., Bringi, V. N., Cifelli, R., Hudak, D. and Petersen, W. A., 2010: A Methodology to Derive Radar Reflectivity‐Liquid Equivalent Snow Rate Relations Using C-Band Radar and a 2D Video Disdrometer. *J. Atmos. Oceanic Technol.*, **27**, 637-651.

Huang, G., V.N. Bringi, D. Moisseev, W.A. Petersen, L. Bliven and D. Hudak, 2015: Use of 2D-video disdrometer to derive mean density–size and Ze–SR relations: Four snow cases from the light precipitation validation experiment, *Atmos. Res.*, **153**, 34–48.

Kuo, K-S, W. S. Olson, B. T. Johnson, M. Grecu, L. Tian, T. L. Clune, B. H. van Aartsen, A. J. Heymsfield, L. Liao, and R. Meneghini, 2016: The microwave radiative properties of falling snow derived from realistic ice particle models. Part I: An extensive database of simulated pristine crystals and aggregate particles, and their scattering properties. *J. Appl. Meteorol. Climatol*.,.55, 691-708.

Liao, L., R. Meneghini, H. Nowell and G. Liu, 2013:Scattering computations of snow aggregates from simple geometrical particle models. *IEEE J. Selected Topics in Earth Obs. and Remote Sens*., **6**, 1409-1417.

Liu, G., 2004: Approximation of single scattering properties of ice and snow particles for high microwave frequencies. *J. Atmos. Sci.*, **61**, 2441-2456.

Liu, G., 2008: A database of microwave single-scattering properties for non spherical ice particles. *Bull. Am. Meteorol. Soc*., **89**, 1563-1570.

590 Locatelli, J., and P. Hobbs, 1974: Fall speeds and masses of solid precipitation particles. *J.*
591 *Geophys. Res.*, **79**, 2185-2197.
592
593 Magono C., and T. Nakamura, 1965: Aerodynamic studies of falling snowflakes, *J. Meteorol.*
594 *Soc. Jpn.*, 43, 139–147.
595
596 Matrosov, S. Y., 1998: A dual-wavelength radar method to measure snowfall rate. *J. Appl.*
597 *Meteor.*, **37**, 1510–1521.
598
599 Matrosov, S. Y., A. J. Heymsfield, and Z. Wang, 2005: Dual-frequency ratio of non-spherical
600 atmospheric hydrometeors. *Geophys. Res. Lett.*, **32**, L13816, doi:10.1029/2005GL023210.
601
602 Mitchell, D. L., R. Zhang, and R. L. Pitter, 1990: Mass-dimensional relations for ice particles
603 and the influence of riming on snowfall rates. *J. Appl. Meteor*., **29**, 153-163.
604
605 Nakaya, U., 1954: *Snow Crystals: Natural and Artificial*. Harvard University Press, 510pp.
606
607 Newman, A., P. A. Kucera, and L. Bliven, 2009: Presenting the snow video imager. *J. Atmos.*
608 *Ocean*. Technol., **26**, 167-179.
609
610 Nowell, H., G. Liu, and R. Honeyager, 2013: Modeling the microwave single-scattering
611 properties of aggregate snowflakes. *J. Geophys. Res. Atmos*., **118**, 7873–7885.
612 doi:10.1002/jgrd.50620.
613
614 Petty, G. W., and W. Huang, 2010: Microwave backscattering and extinction by soft ice spheres
615 and complex snow aggregates. *J. Atmos. Sci*., **67**, pp. 769-787.
616
617 Seto, S, T. Iguchi, and T. Oki, 2013: The basic performance of a precipitation retrieval algorithm
618 for the global precipitation measurement mission's single/dual-frequency radar
619 measurements. *IEEE Trans. Geosci. Remote Sens.*, **51**, 5239–5251.
620
621 Szyrmer, W., and I. Zawadzki, 2014a: Snow studies. Part III: Theoretical derivations for the
622 ensemble retrieval of snow microphysics from dual-wavelength vertically pointing radars. *J.*
623 *Atmos. Sci.,***71,** 1158–1170.
624
625 Szyrmer, W., and I. Zawadzki, 2014b: Snow studies. Part IV: Ensemble retrieval of snow
626 microphysics from dual-wavelength vertically pointing radars. *J. Atmos. Sci.,***71,** 1172–1186.
627
628 Wang, Z., G. M. Heymsfield, L. Li, and A. J. Heymsfield, 2005: Retrieving optically thick ice
629 cloud microphysical properties by using airborne dual-wavelength radar measurements. *J.*
630 *Geophys. Res.*, **110**, D19201, doi:10.1029/2005JD005969.
631
632 Weinman, J., and M.-J. Kim, 2007: A simple model of the millimeter-wave scattering parameters
633 of randomly oriented aggregates of finite cylindrical ice hydrometeors. *J. Atmos. Sci.*, **64**,
634 634-644.
635

636 Zikmunda, J., and G. Vali, 1972: Fall patterns and fall velocities of rimed ice crystals. *J. Atmos.*
637 *Sci*., **29**, 1334-1347.
638

639 Table 1 Snow events during winter of 2014 in Wallops Island, Virginia

640

Events	Start Time (UTC)	End Time (UTC)	Accumulation (mm)	Mean Temperature (^{0}C)
1	JAN0305:09	JAN03 11:30	46.41	-1.4
2	JAN21 22:05	JAN22 10:03	5.52	-5.4
3	JAN28 20:41	JAN29 12:40	62.12	-9.5
4	FEB14 01:58	FEB14 05:12	6.37	1.9
5	FEB15 20:41	FEB15 23:23	0.76	2.2
6	MAR03 14:40	MAR03 22:00	34.15	-4.4
7	MAR17 08:04	MAR17 20:53	20.93	0.8
8	MAR25 18:50	MAR26 06:13	47.40	1.0

641

Figure captions:

Fig.1 Comparisons of backscattering (left) and extinction (right) coefficients of 3 snow aggregates with the results from the sphere, oblate and prolate spheroids at a frequency of 35.6 GHz in terms of equivalent ice diameter. A constant snow density of 0.2 g/cm^3 is assumed for all spherical and spheroidal particle models. The oblate and prolate spheroids are randomly oriented with aspect ratios (γ) of 0.5 and 2, respectively.

Fig.2 Backscattering (left) and extinction (right) coefficients from the scattering database (blue dots), simple scattering model (red curves), which is the randomly-oriented oblate spheroid with a constant effective density of 0.2 g/cm^3 and an aspect ratio of 0.7, and scattering-database-simple-model-combined results (black curves), also referred to as "fitted", at Ku band. The mean values of the scattering results are used for the combined results over the data range.

Fig.3 Backscattering (left) and extinction (right) coefficients from the scattering database (blue dots), simple scattering model (red curves), which is the randomly-oriented oblate spheroid with a constant effective density of 0.2 g/cm^3 and an aspect ratio of 0.7, and scattering-database-simple-model-combined results (black curves), also referred to as "fitted", at Ka band. The mean values of the scattering results are used for the combined results over the data range.

Fig.4 The differential frequency ratio (DFR=$10LOG_{10}(Z_{Ku}/Z_{Ka})$) as a function of equivalent-liquid median mass diameter D_m. (Left): DFR-D_m relations are plotted with several effective snow densities (ρ_s) from 0.1 to 0.4 g/cm^3 as the shape factor (μ) of the gamma PSD is set to zero and the aspect ratio (γ) of the oblate spheroid particles is set to 0.7. (Middle): DFR-D_m relations are plotted with the aspect ratios of 0.5, 0.7 and 1 at ρ_s=0.2 g/cm^3 and μ=0. (Right): DFR-D_m relations are plotted with the values of μ of 0, 3 and 6 at ρ_s=0.2 g/cm^3 and γ=0.7.

Fig.5 The retrieval look-up tables that show the snow water content (SWC) (top-left) and equivalent snowfall rate (R_S) (top-right), both of which are normalized by the Ku-band radar reflectivity factor (Z_{Ku}), as a function of the DFR, defined by $10LOG_{10}(Z_{Ku}/Z_{Ka})$, for several effective snow densities (ρ_s) with the values from 0.05 to 0.5 g/cm^3. The liquid equivalent median mass diameter D_m (bottom-left) and the PSD scale parameter N_w normalized by Z_{Ku} (bottom-right) are also plotted in terms of DFR.

Fig.6 Flowchart of computing radar parameters and snow size and bulk properties.

Fig.7 The look-up tables used for the retrieval of SWC (left) and R_S (right) with μ of 0, 3 and 6, respectively, as computed from the single scattering tables depicted in Figs.2-3.

Fig.8 Example of a segment of the PSD measurements (1000 minutes) in time series taken from 8 snow events during winter of 2014 at the NASA Wallops Flight Facility using the SVI/PIP. The particle size spectra (mm^{-1} m^{-3}), shown in the color scale, are given in the top panel while equivalent snow fall rate and actual median mass diameter are displayed in the middle and

677 bottom panels, respectively. The PSD data, obtained by averaging the measurements over 1-
678 minute integration time, are merged from all the snow events into one data file with consecutive
679 time.

680 Fig.9 The snow water content (SWC) (top row) and equivalent snowfall rate (R_S) (bottom row),
681 both of which are normalized by the Ku-band radar reflectivity factor (Z_{Ku}), as a function of the
682 DFR, defined by $10LOG_{10}(Z_{Ku}/Z_{Ka})$, for several effective snow densities (ρ_s) with the values
683 from 0.05 to 0.5 g/cm^3. The scatter plots (red dots) are the results derived from the measured
684 PSD that were collected by the SVP/PIP from 8 snow events in the winter of 2014 at the NASA
685 Wallops Flight Facility. Two empirical density-size relationships reported by Brandes et al.
686 (2007) and Heymsfield et al. (2010) are used in converting the measured PSD to the snow mass
687 spectra, and the results from their respective relations are shown in the left and right panels.

688 Fig.10 Flowchart detailing the procedures of obtaining radar reflectivities and snow parameters.

689

690

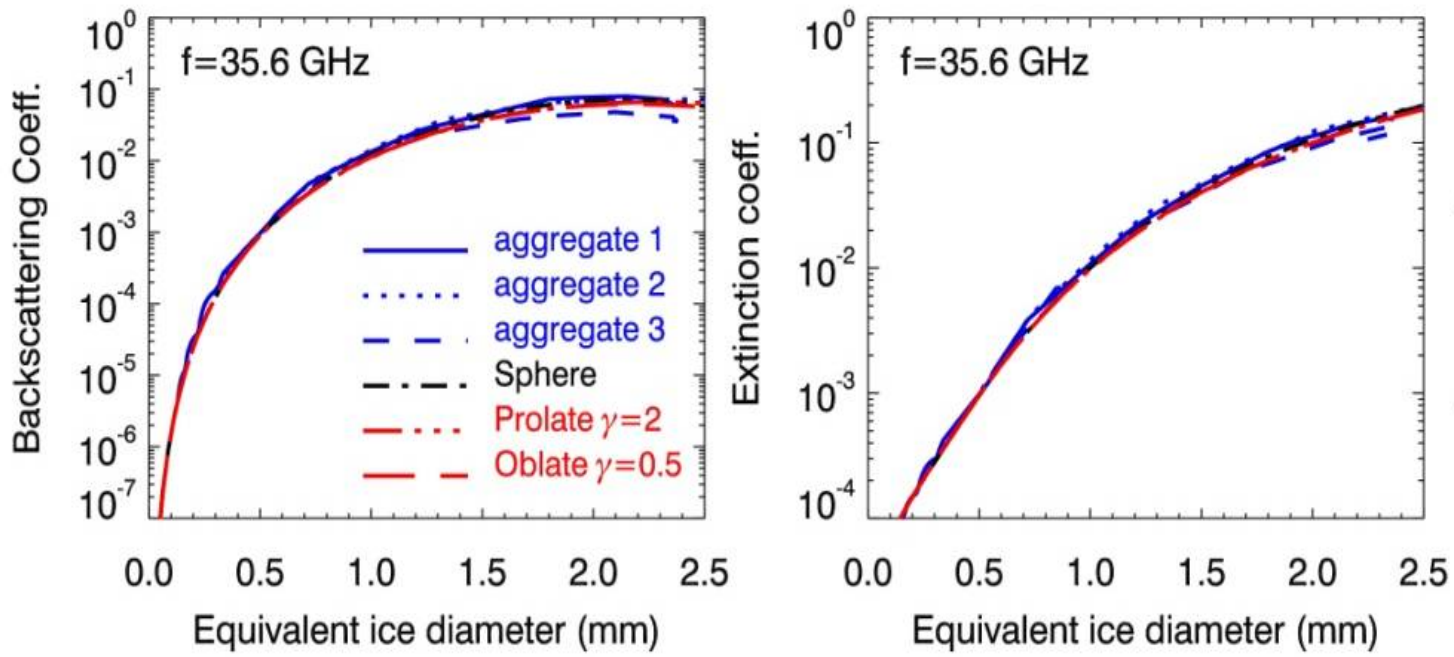

Fig.1 Comparisons of backscattering (left) and extinction (right) coefficients of 3 snow aggregates with the results from the sphere, oblate and prolate spheroids at a frequency of 35.6 GHz in terms of equivalent ice diameter. A constant snow density of 0.2 g/cm^3 is assumed for all spherical and spheroidal particle models. The oblate and prolate spheroids are randomly oriented with aspect ratios (γ) of 0.5 and 2, respectively.

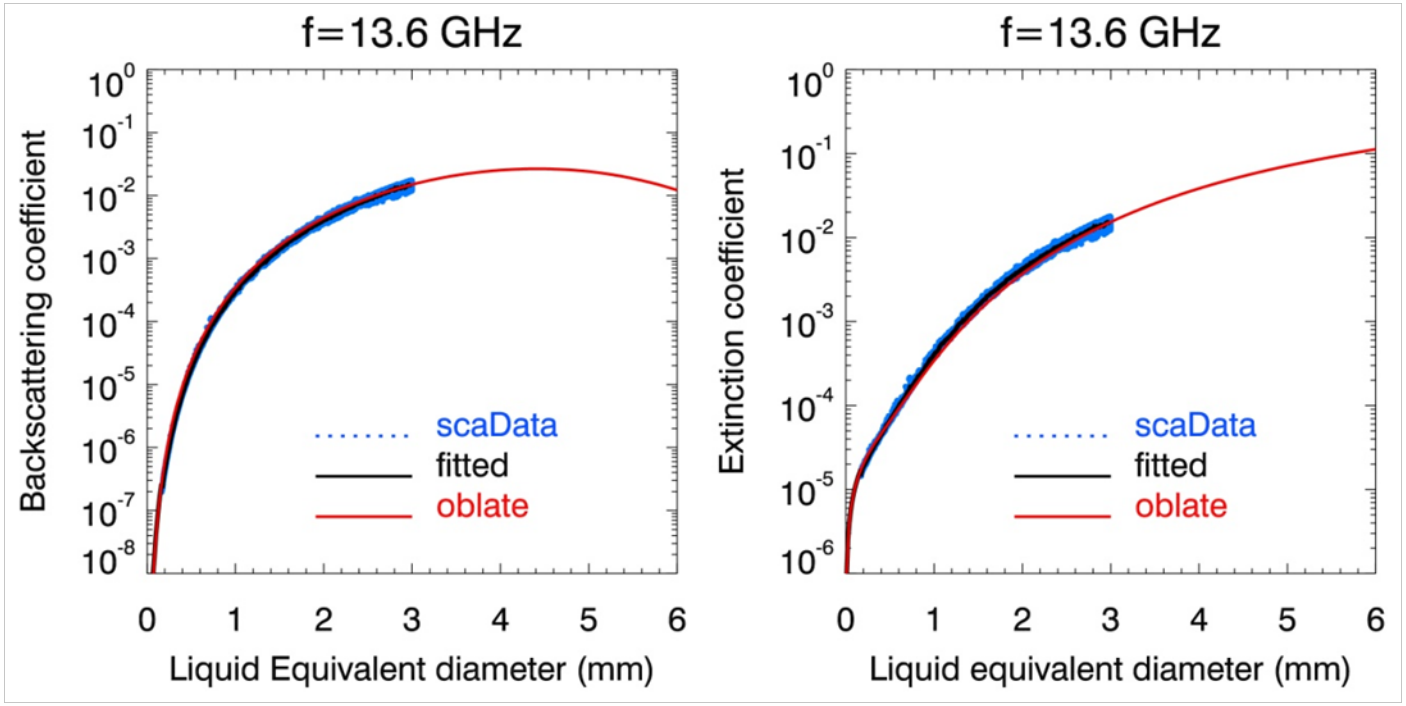

Fig.2 Backscattering (left) and extinction (right) coefficients at Ku-band from the scattering database (blue dots), simple scattering model (red curves), which is the randomly-oriented oblate spheroid with a constant effective density of 0.2 g/cm^3 and an aspect ratio of 0.7, and scattering-database-simple-model-combined results (black curves), also referred to as "fitted". The mean values of the scattering results are used for the combined results over the data range.

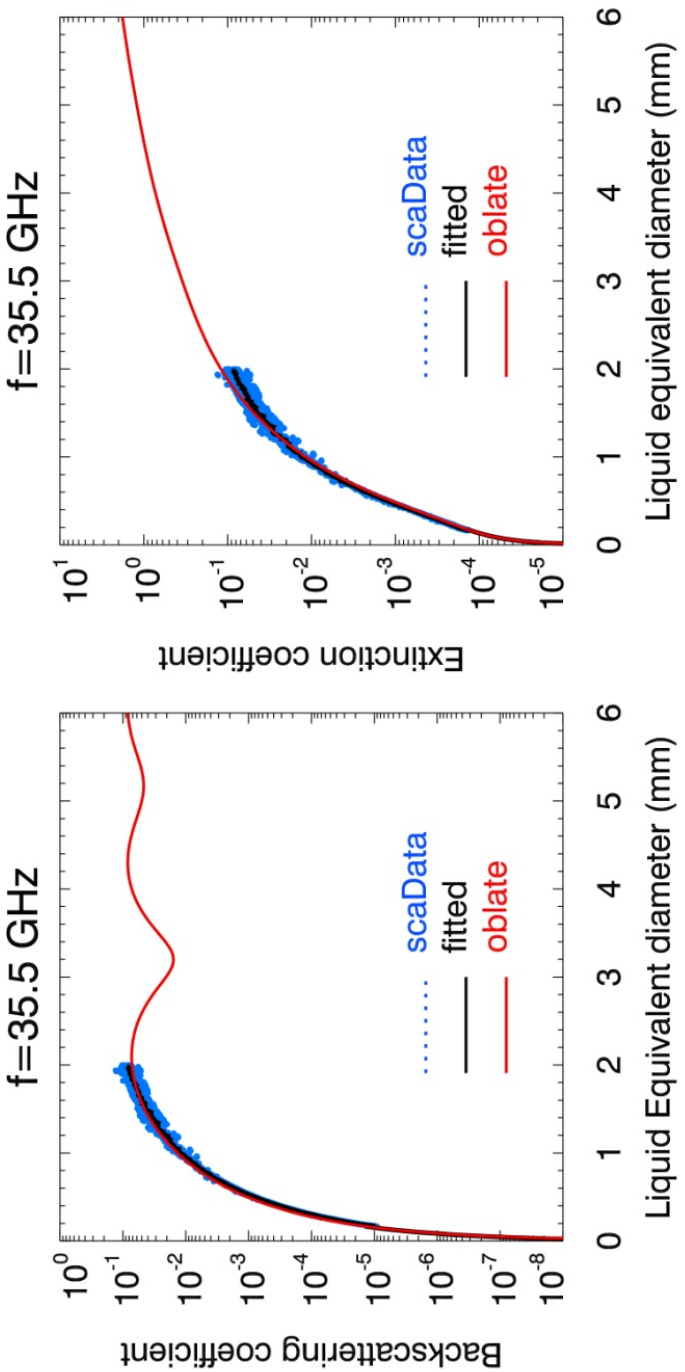

Fig.3 Backscattering (left) and extinction (right) coefficients from the scattering database (blue dots), simple scattering model (red curves), which is the randomly-oriented oblate spheroid with a constant effective density of 0.2 g/cm^3 and an aspect ratio of 0.7, and scattering-database-

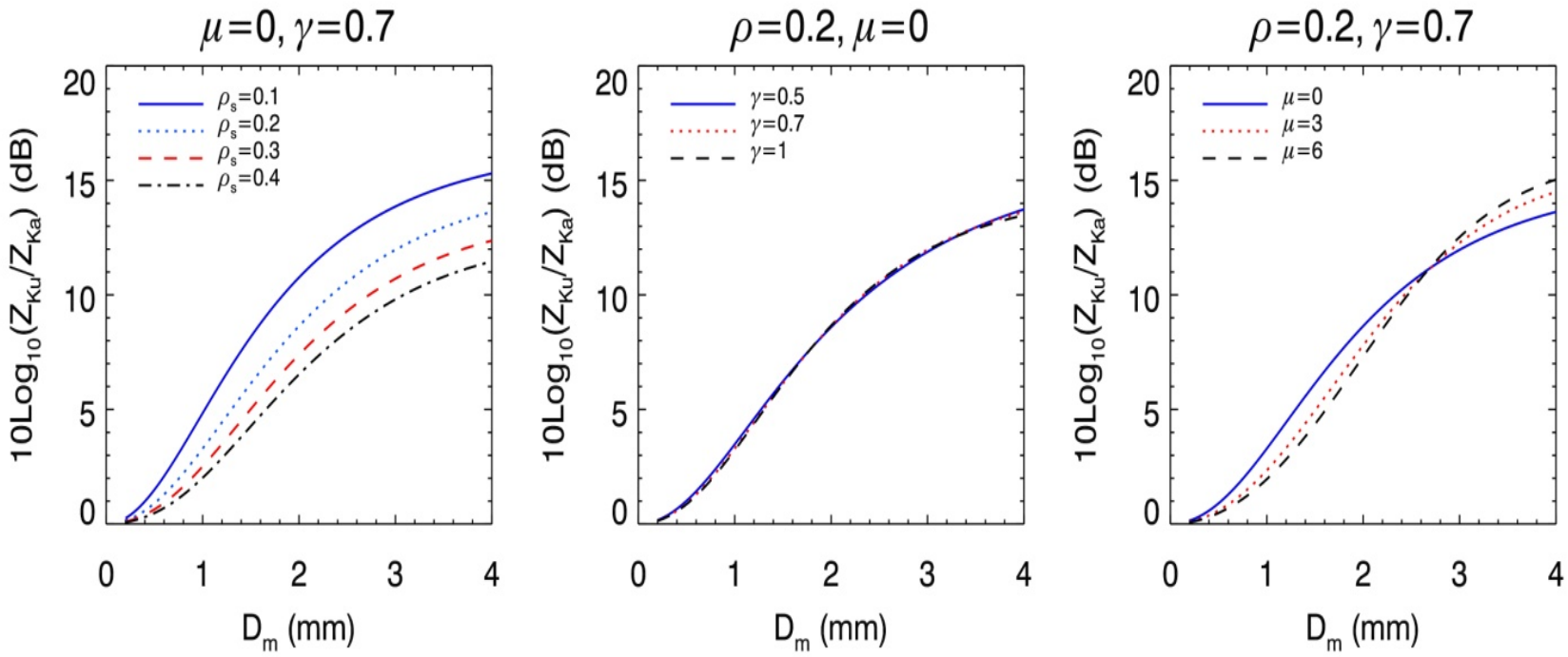

Fig.4 The differential frequency ratio (DFR=$10LOG_{10}(Z_{Ku}/Z_{Ka})$) as a function of equivalent-liquid median mass diameter D_m. (Left): DFR-D_m relations are plotted with several effective snow densities (ρ_s) from 0.1 to 0.4 g/cm^3 as the shape factor (μ) of the gamma PSD is set to zero and the aspect ratio (γ) of the oblate spheroid particles is set to 0.7. (Middle): DFR-D_m relations are plotted with the aspect ratios of 0.5, 0.7 and 1 at ρ_s=0.2 g/cm^3 and μ=0. (Right): DFR-D_m relations are plotted with the values of μ of 0, 3 and 6 at ρ_s=0.2 g/cm^3 and γ=0.7.

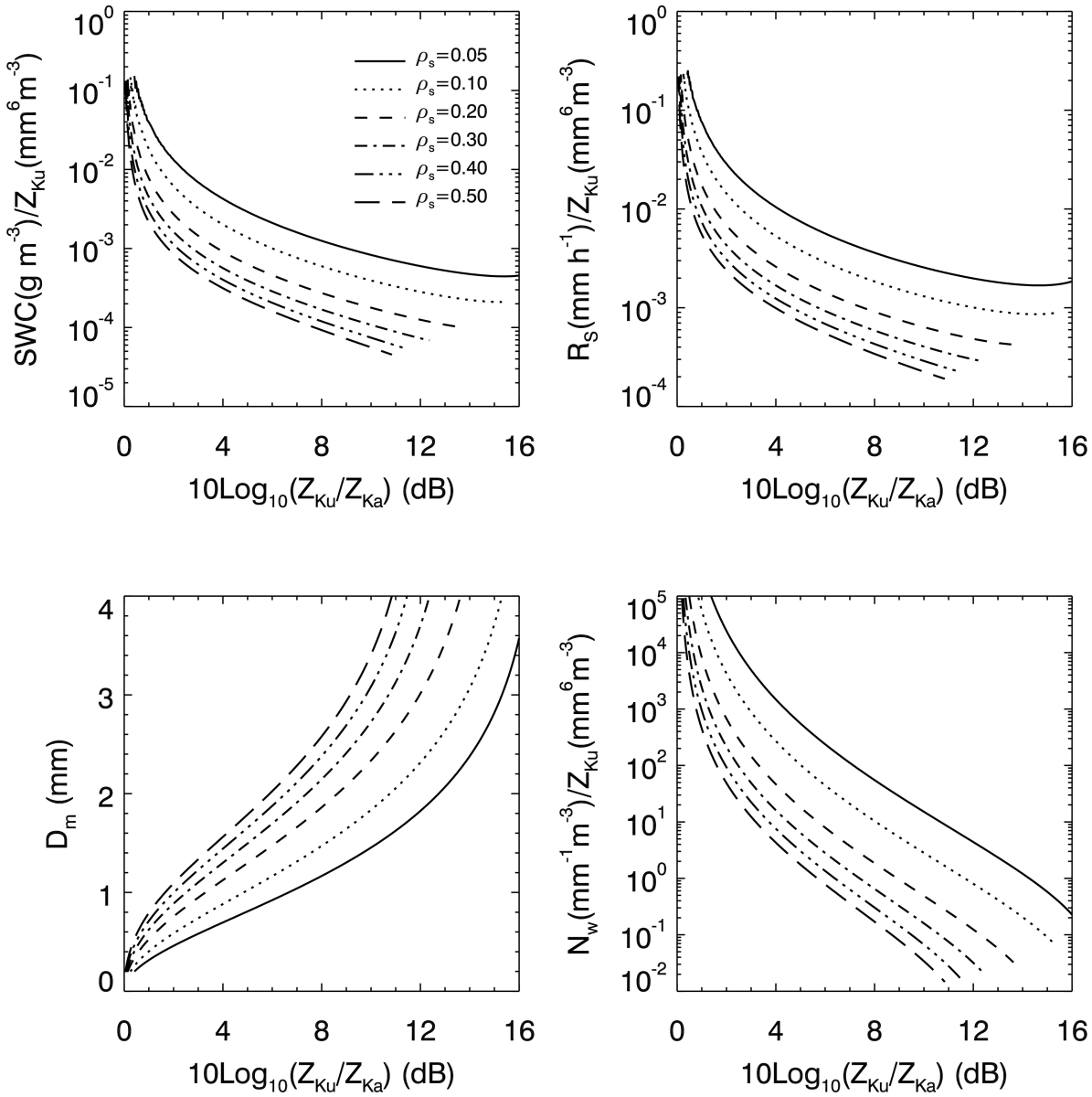

723

724

725

726 Fig.5 The retrieval look-up tables that show the snow water content (SWC) (top-left) and
727 equivalent snowfall rate (R_S) (top-right), both of which are normalized by the Ku-band radar
728 reflectivity factor (Z_{Ku}), as a function of the DFR, defined by $10LOG_{10}(Z_{Ku}/Z_{Ka})$, for several
729 effective snow densities (ρ_s) with the values from 0.05 to 0.5 g/cm^3. The liquid equivalent
730 median mass diameter D_m (bottom-left) and the PSD scale parameter N_w normalized by Z_{Ku}
731 (bottom-right) are also plotted in terms of DFR.

732

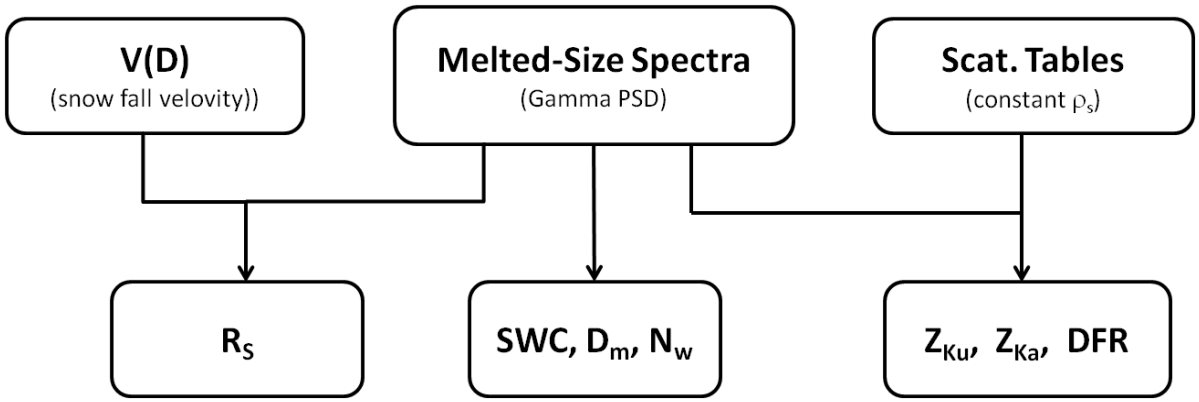

733

734

735 Fig.6 Flowchart of computing radar parameters and snow size and bulk properties.

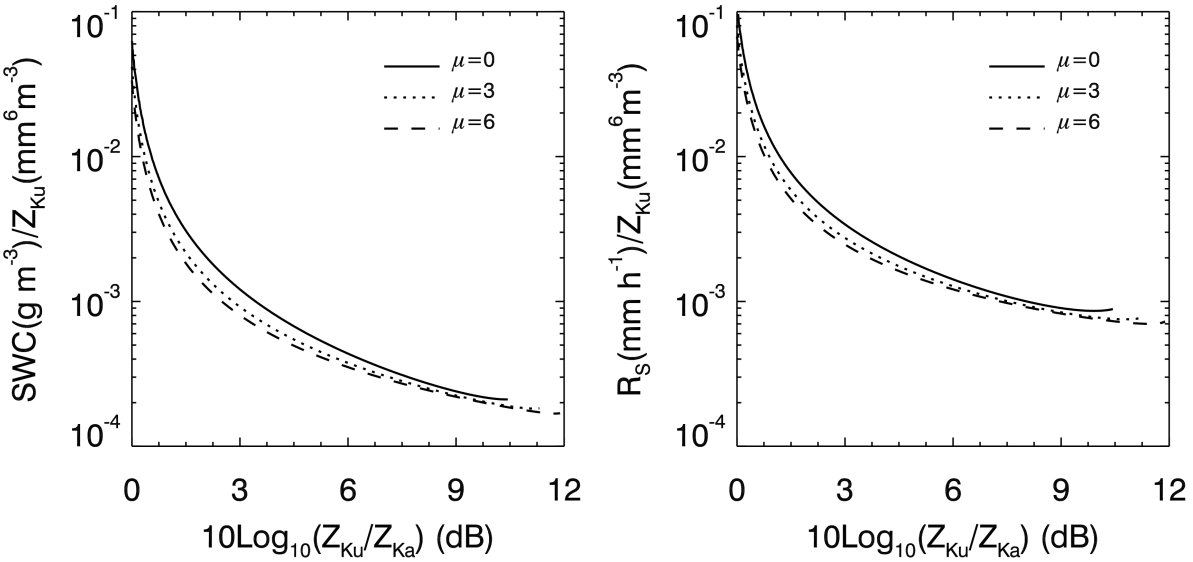

Fig.7 The look-up tables used for the retrieval of SWC (left) and R_S (right) with μ of 0, 3 and 6, respectively, as computed from the single scattering tables depicted in Figs.2-3.

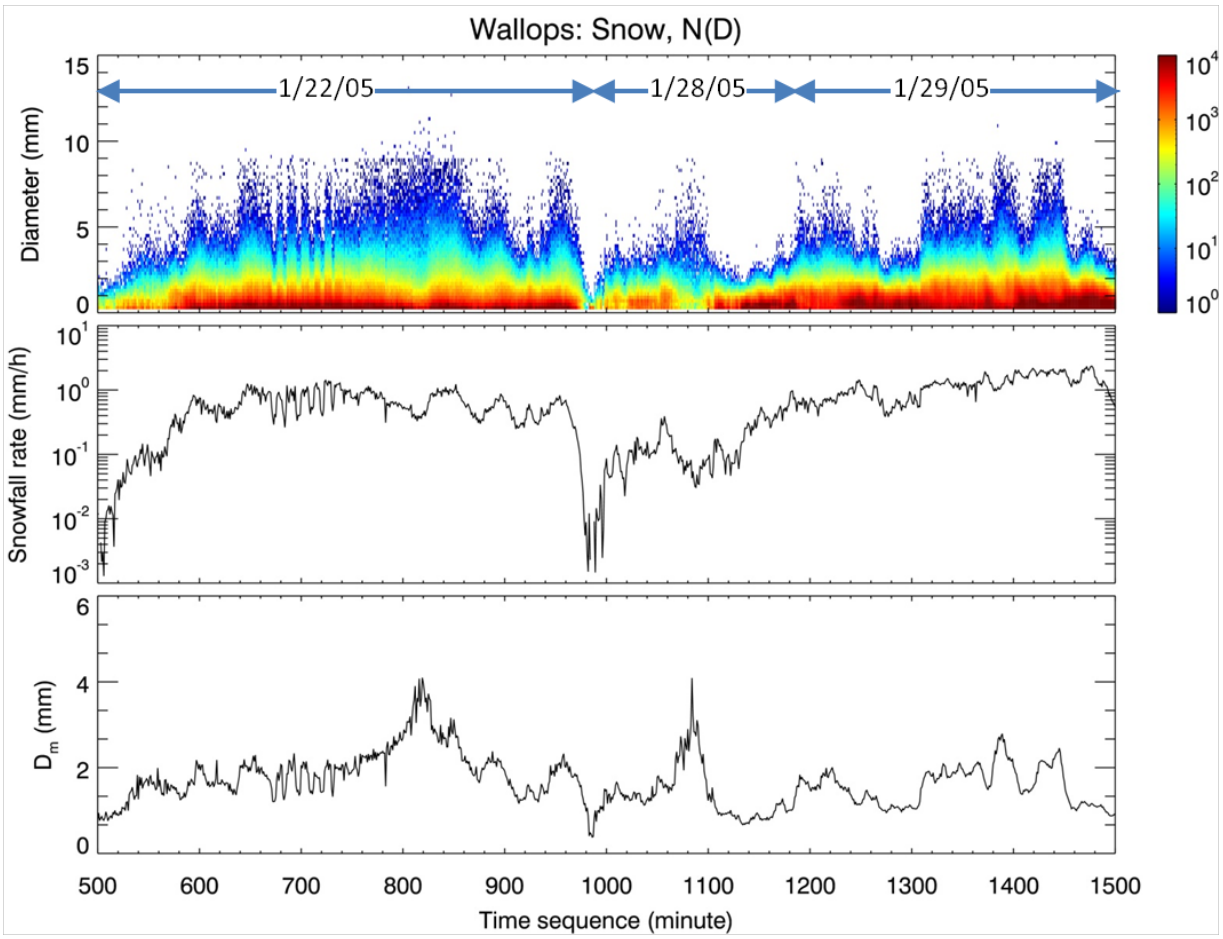

Fig.8 Example of a segment of the PSD data, obtained by averaging the measurements over 1-minute integration time, in time series taken from 8 snow events during winter of 2014 at the NASA Wallops Flight Facility using the SVI/PIP. The particle size spectra (mm^{-1} m^{-3}), shown in the color scale, are given in the top panel while equivalent snow fall rate and actual median mass diameter are displayed in the middle and bottom panels, respectively. The dates provided in the top panel correspond to the snow events displayed.

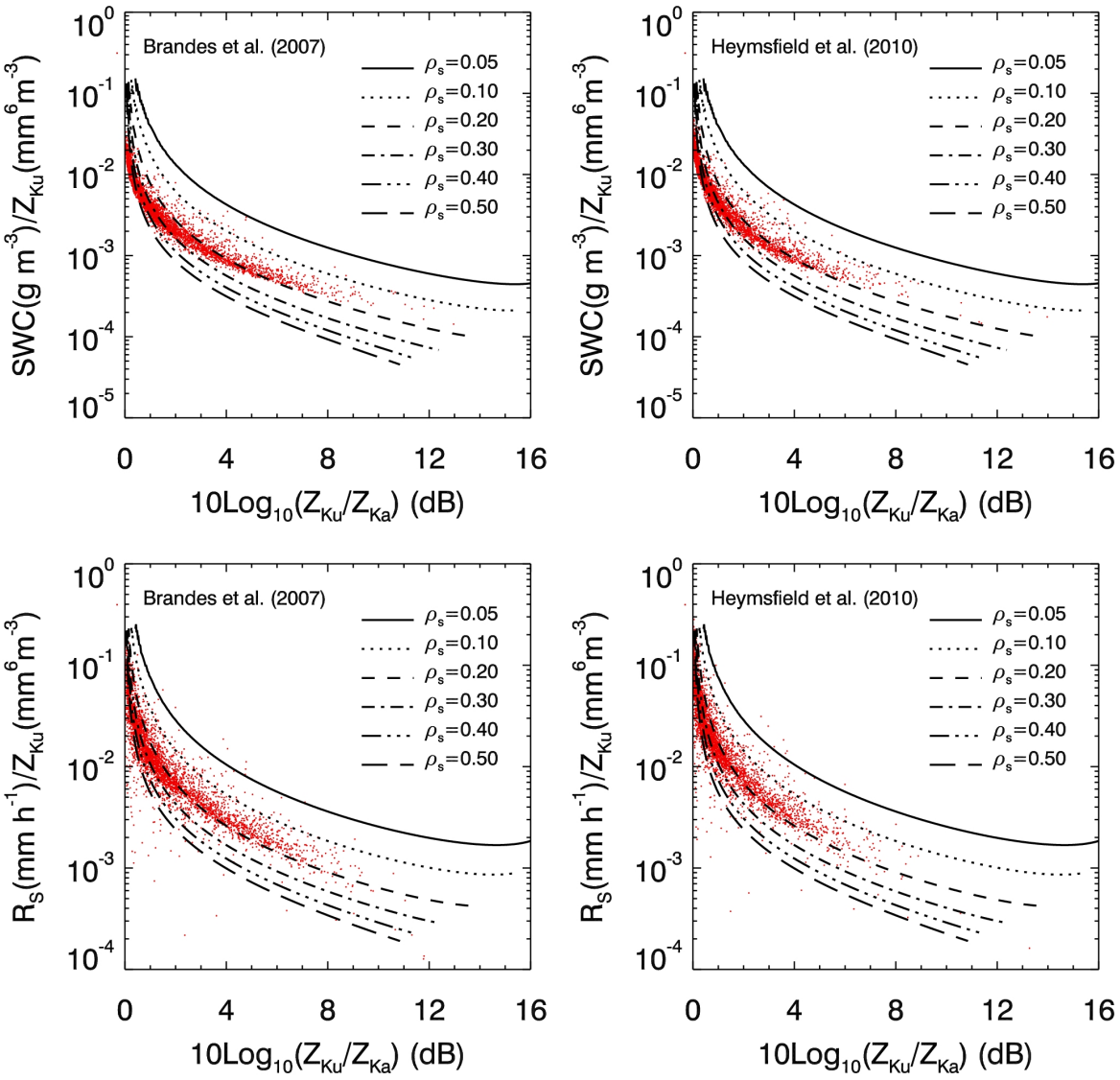

758

759 Fig.9 The snow water content (SWC) (top row) and equivalent snowfall rate (R_S) (bottom row),
760 both of which are normalized by the Ku-band radar reflectivity factor (Z_{Ku}), as a function of the
761 DFR, defined by $10LOG_{10}(Z_{Ku}/Z_{Ka})$, for several effective snow densities (ρ_s) with the values
762 from 0.05 to 0.5 g/cm^3. The scatter plots (red dots) are the results derived from the measured
763 PSD that were collected by the SVP/PIP from 8 snow events in the winter of 2014 at the NASA
764 Wallops Flight Facility. Two empirical density-size relationships reported by Brandes et al.
765 (2007) and Heymsfield et al. (2010) are used in converting the measured PSD to the snow mass
766 spectra, and the results from their respective relations are shown in the left and right panels.

767

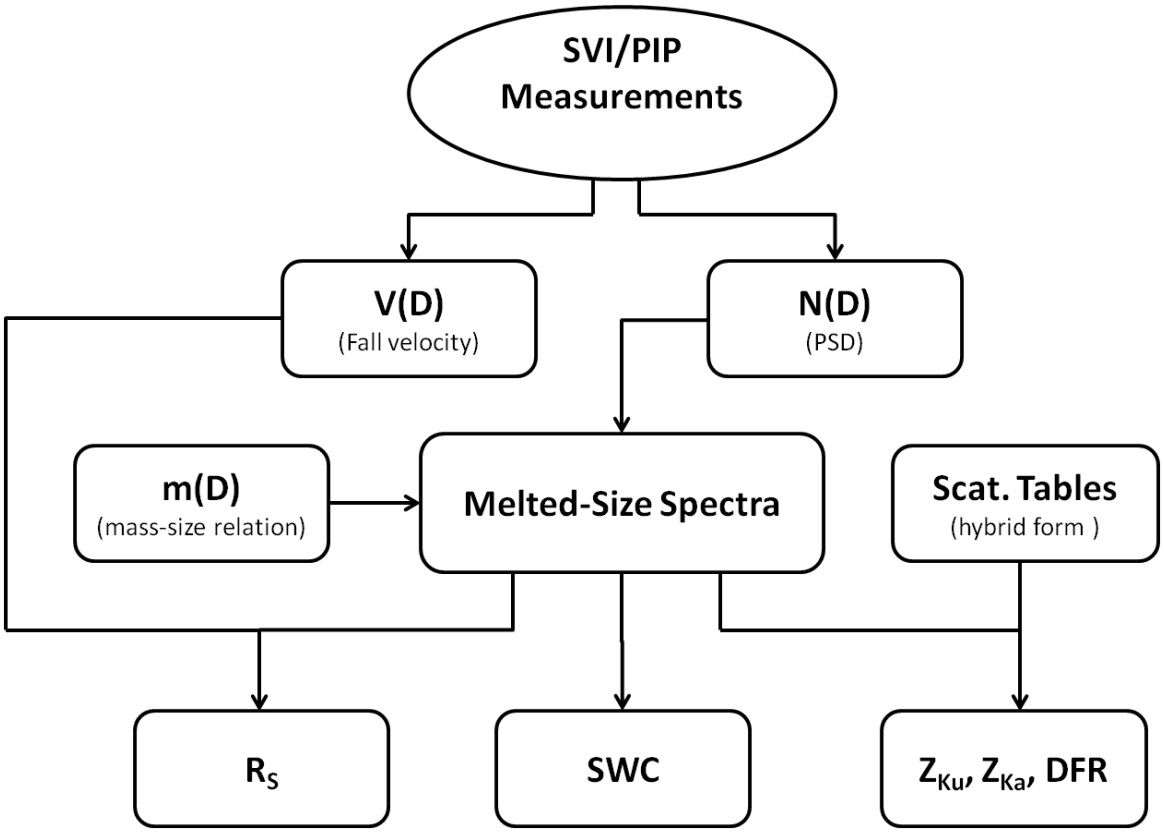

768

769

770 Fig.10 Flowchart detailing the procedures of obtaining radar reflectivities and snow parameters.

771